ARTICLE IN PRESS

International Journal of Plasticity xxx (2012) xxx–xxx

Contents lists available at SciVerse ScienceDirect

International Journal of Plasticity

journal homepage: www.elsevier.com/locate/ijplas

# Transformation and slip behavior of $Ni_2FeGa$

H. Sehitoglu [a,*], J. Wang [a], H.J. Maier [b]

[a] Department of Mechanical Science and Engineering, University of Illinois at Urbana-Champaign, 1206 W. Green St., Urbana, IL 61801, USA
[b] University of Paderborn, Lehrstuhl für Werkstoffkunde, D-33095 Paderborn, Germany

ARTICLE INFO

*Article history:*
Received 12 March 2012
Received in final revised form 28 May 2012
Available online xxxx

*Keywords:*
Shape memory
Dislocation slip
Phase transformation
Energy barrier
Pseudoelasticity

ABSTRACT

$Ni_2FeGa$ is a relatively new shape memory alloy (SMA) and exhibits superior characteristics compared to other SMAs. Its favorable properties include low transformation stress, high reversible strains and small hysteresis. The first stage of stress-induced martensitic transformation is from a cubic to a modulated monoclinic phase. The energy barriers associated with the transformation from $L2_1$ (cubic) to modulated martensite (10M-martensite) incorporating shear and shuffle are established via atomistic simulations. In addition, the slip resistance in the [111] direction and the dissociation of full dislocations into partials as well as slip in the [001] direction are studied. The unstable stacking fault energy barriers for slip by far exceeded the transformation transition state barrier permitting transformation to occur with little irreversibility. Experiments at the meso-scale on single crystals and transmission electron microscopy were conducted to provide further proof of the pseudoelastic (reversible) behavior and the presence of anti-phase boundaries. The results have implications for design of new shape memory alloys that possess low energy barriers for transformation coupled with high barriers for dislocation slip.



## 1. Introduction

### 1.1. Challenges in Designing Shape Memory Alloys

Designing new shape memory materials that exhibit superior transformation characteristics remains a challenge. There needs to be a better fundamental basis for describing how reversible transformation (shape memory) works in the first place. Specifically, two aspects remain uncertain. The first is that the phase changes involve complex transformation paths with shear and shuffle (Ahlers, 2002) and the energy barrier levels corresponding to the transition are not well established. The second issue is that the determination of dislocation slip resistance (Olson and Cohen, 1975), which decides the reversibility of transformation of shape memory alloys, is very important and requires further study. Thus, this paper is geared towards establishing both the energy barriers in the phase changing of $Ni_2FeGa$ and the fault energies associated with dislocation slip for the same material.

Thermo-elastic phase transformation refers to a change in lattice structure upon exposure to stress or temperature and return of the lattice to the original state upon removal of stress or temperature (Delaey et al., 1974). Modern understanding of shape memory transforming materials has relied on the phenomenological theory of the martensitic transformation (Wechsler et al., 1953), which does not deal with the presence of dislocation slip. The presence of slip has been observed in experimental work at micro- and meso-scales (Otsuka and Wayman, 1998; Duerig et al., 1990), and incorporated in some of the continuum modeling approaches (Boyd and Lagoudas, 1996). A low transformation stress (Sehitoglu et al., 2000) and

* Corresponding author.
*E-mail address:* huseyin@illinois.edu (H. Sehitoglu).

0749-6419/$ - see front matter © 2012 Elsevier Ltd. All rights reserved.
http://dx.doi.org/10.1016/j.ijplas.2012.05.011

high slip resistance (Hamilton et al., 2004) are precursors to reversible martensitic transformation. Recently, theoretical developments at atomic length scales have been utilized (Hatcher et al., 2009; Kibey et al., 2009; Wagner and Windl, 2008) bringing into light the magnitude of energies of different phases and defect fault energies in NiTi.

NiTi is the most well known shape memory alloy that meets the requirement of excellent slip resistance in both martensite (Ezaz et al., 2011) and in austenite (Manchiraju and Anderson, 2010; Moberly et al., 1991; Norfleet et al., 2009; Pelton et al., 2012; Simon et al., 2010). The recent interest in the austenite slip behavior of NiTi is well founded because it is a key factor that influences the shape memory response.

We note that some of the other shape memory alloys of the Cu-variety (Damiani et al., 2002b; Malarria et al., 2009; Roqueta et al., 1997; Sade et al., 1988; Sittner et al., 1998) and the Fe-based (Maki, 1998a,b; Morito et al., 2000; Jost, 1999; Tsuzaki et al., 1992) alloys possess large transformation strains but are susceptible to plastic deformation by slip. Plastic deformation has been incorporated into continuum energy formulations where the interaction of plastic strains and the transformation improves the prediction of overall mechanical response (Bartel et al., 2011; Idesman et al., 2000; Levitas, 2002). All these previous works point to the importance of dislocation slip resistance in shape memory alloys.

The $Ni_2FeGa$ alloys have large recoverable strains (Chumlyakov et al., 2008; Hamilton et al., 2007a,b) and can potentially find some important applications like NiTi. In the case of $Ni_2FeGa$ alloys, stress-induced transformation to modulated martensite (Masdeu et al., 2005; Omori et al., 2004; Santamarta et al., 2006a,b; Sutou et al., 2004) and the slip deformation of austenite (Hamilton et al., 2007a,b) are two factors that dictate shape memory performance. The phase change in $Ni_2FeGa$ occurs primarily upon shape strains (Bain strain) in combination with shuffles to create a 'modulated' martensitic structure. The 'modulated' monoclinic structure has a lower energy than the 'non-modulated' lattice, and hence is preferred. We focus on atomic movements and the energy landscapes for transformation of $L2_1$ austenite to a 10M modulated martensite structure and establish the barrier for this change. We then investigate the dislocation slip barriers in [111] and [001] directions.

It is important to assess the transformation paths and energies associated with the austenite to martensite transformation simultaneously with dislocation slip behavior because the external shear stress that can trigger transformation can also result in dislocation slip. What we show is that the order strengthened $Ni_2FeGa$ alloy requires elevated stress levels for dislocation slip while undergoing transformation nucleation at much lower stress magnitudes (with lower energy barriers).

### 1.2. Energetics of Phase Transformation and Dislocation Slip

A schematic of pseudoelastic stress-strain response at constant temperature is given in Fig. 1. We note that the initial crystal structure at zero strain is that of austenite. Upon deformation, the crystal undergoes a phase transformation to a modulated martensitic structure. In the case of $Ni_2FeGa$, the structures of austenite and martensite are cubic and monoclinic, respectively. Over the plateau stress region, austenite and martensite phases can coexist. In the vicinity of austenite to martensite interfaces, high internal stresses are generated to satisfy compatibility. Hence, slip deformation can occur in the austenite domains as illustrated in the schematic. Once the transformation is complete, the deformation of the martensitic phase occurs with an upward curvature. Upon unloading, the martensite reverts back to austenite as shown in the schematic. The strain recovers at the macroscale, but at the micro-scale residual slip deformation could remain as shown with TEM studies.

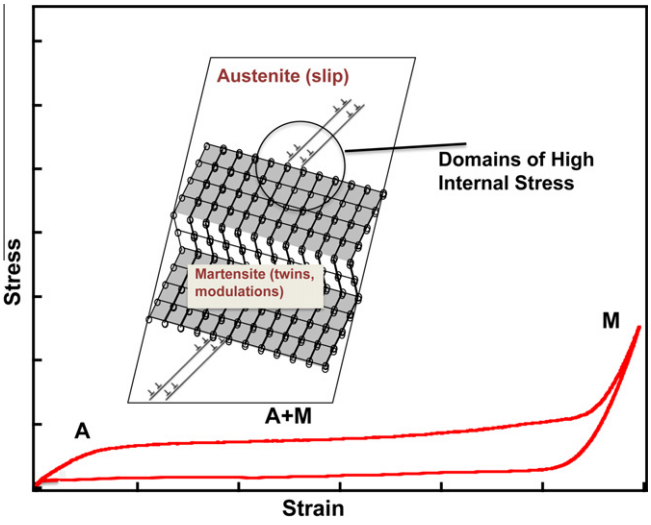


**Fig. 1.** Schematic of stress–strain curve displaying the modulated martensite and dislocation slip in austenite over the plateau region during pseudoelasticity.

Please cite this article in press as: Sehitoglu, H., et al. Transformation and slip behavior of $Ni_2FeGa$. Int. J. Plasticity (2012), http://dx.doi.org/10.1016/j.ijplas.2012.05.011

We capture the energetics of the transformation through *ab initio* density functional theory (DFT) calculations. In Fig. 2(a), the initial lattice constant is $a_o$ and the monoclinic lattice constants are a, b and c with a monoclinic angle. We incorporate shears and shuffles for the case of transformation from $L2_1$ to 10M. A typical transformation path is described in Fig. 2(a). The martensite has lower energy than the austenite. To reach the martensitic state, there exists an energy barrier (corresponding to $\gamma_u^{A\to M}$ in Fig. 2(a)) that needs to be overcome. This barrier is dictated by the energy at the transition state (TS) as shown in Fig. 2(a). A smaller barrier is desirable to allow transformation at stress levels well below dislocation mediated plasticity. Along the transformation path, we find a rather small energy barrier (8.5 mJ/m$^2$ for the $L2_1$ to 10M transformation in $Ni_2FeGa$).

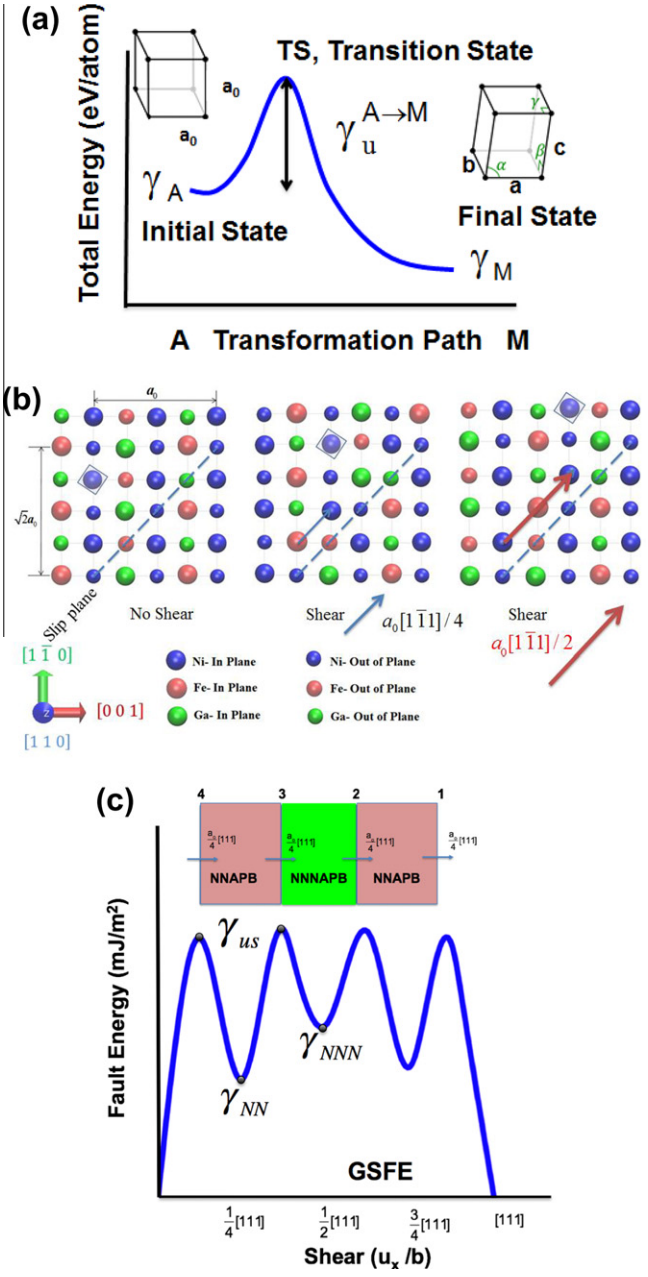


**Fig. 2.** (a) Schematic of transformation path showing the energy in the initial state, the final state and the transition state, (b) atomic arrangements of $Ni_2FeGa$ with long range order (first configuration). The viewing direction is [110]. The (001) planes are made of all Ni atoms, and alternating Fe and Ga atoms. The dashed line represents the slip plane. The displacement <111>/4 creates nearest neighbor APBs (middle configuration) and the displacement <111>/2 results in next nearest neighbor APBs (third configuration). (c) Generalized fault energy of austenite associated with full dislocation dissociation into partials in an ordered alloy.

Please cite this article in press as: Sehitoglu, H., et al. Transformation and slip behavior of $Ni_2FeGa$. Int. J. Plasticity (2012), http://dx.doi.org/10.1016/j.ijplas.2012.05.011

Dislocation slip resistance in the $L2_1$ austenite can be understood by consideration of energetics of slip displacements in the [111] direction associated with the motion of the dissociated dislocations. Ribbons of anti-phase boundaries (APBs) form by dissociation of superdislocations in the $L2_1$ parent lattice. We compute the separation distance of the superpartials via equilibrium considerations and show the presence of these APBs from TEM observations. The energy barriers are manifested via generalized stacking fault energy curves (GSFE) and decide the slip resistance of the material. We check the GSFE curves in two possible dislocation slip systems and calculate theoretical resolved shear stress.

The fundamental descriptions of the APB formation in ordered cubic materials point to decomposition of full dislocations (Koehler and Seitz, 1947; Marcinkowski and Brown, 1961). For the $Ni_2FeGa$, as atoms are sheared over other atoms in neighboring planes the energy landscape indicates the decomposition of the full dislocation to four partials resulting in APBs. The partial dislocations are not zig zag type as in face centered cubic systems but are in the same direction as the full dislocation. This is illustrated in Fig. 2(b). It is easiest to see the APB formation with a [110] projection (Fig. 2(b)). The x-axis is [001] and the y-axis is $[1\bar{1}0]$ in this case. In this view atoms on only two planes (in-plane and out-of-plane) are noted (a different view will be illustrated later). Because we have twice as many Ni atoms then Fe and Ga, in the $[1\bar{1}0]$ direction every second column has all Ni atoms. When slip occurs with vector 1/4 $[1\bar{1}1]$ the original ordering of the lattice no longer holds. The passage of the first partial 1/4 $[1\bar{1}1]$ results in disordering of the atomic order at near neighbors. The passage of the second partial restores the original stacking of next to near neighbor atoms. Upon a slip displacement of 1/2 $[1\bar{1}1]$ the columns with all Ni atoms are restored but other columns do not have the original ordering (Fig. 2(b)). Upon displacement of $[1\bar{1}1]$ the original lattice structure with long range order of the matrix is recovered. The fault energy barriers corresponding to Fig. 2(b) have several minima (metastable equilibrium points) corresponding to the passages of the partial dislocations (Fig. 2(c)). More details will be given later in the text. In Fig. 2(b) $\gamma_{US}$ refers to the unstable fault energy and $\gamma_{NN}$ and $\gamma_{NNN}$ describe the nearest-neighbor (NN) and next-nearest neighbor (NNN) APB energies respectively. The fault energy barriers are moderately high (>400 $mJ/m^2$ in $Ni_2FeGa$) and point to the considerable slip resistance in $Ni_2FeGa$. We provide TEM evidence of the presence of APBs in the austenitic phase for samples that have undergone pseudoelastic cyclic deformation.

## 2. Fundamentals of Cubic to Modulated (10M) Transformation in $Ni_2FeGa$

The martensitic structure is critical to the properties of ferro-magnetic shape memory alloys. Their tetragonality c/a, twinning stress and magnetocrystalline anisotropy constant determine the magnetic-field-induced strain (MFIS) (Luo et al., 2011b; Morito et al., 2005). However, large MFIS originates mainly from the contribution of the modulated martensites (Han et al., 2007). Experiments have shown that the cubic structure ($L2_1$) undergoes the phase transformation to martensitic phases, designated modulated structure (10M/14M) and tetragonal structure ($L1_0$). The transformation from a cubic structure ($L2_1$) to a modulated 10M structure is an important one in shape memory alloys of the ferro-magnetic variety (Efstathiou et al., 2008; Hamilton et al., 2006, 2007a; Martynov, 1995; Segui et al., 2005). The $Ni_2FeGa$ alloys undergo such a transformation via a combination of shear (distortion) and shuffle. This is the first stage of multiple transformation steps resulting in the $L1_0$ structure. It is a very important step because it decides the transformation stress and the plateau stress for the shape memory alloy.

In Fig. 3(a), the $L2_1$ lattice of Ni-Fe-Ga is shown. We note that the distance $a_o$ represents repeating atom positions in the <001> directions. We refer to coordinates in the $L2_1$ structure with the larger cell noting that the small cell represents a B2 structure. The $L2_1$ unit cell contains eight cells of the B2 type. Upon transformation to martensite, the lattice structure becomes monoclinic (Fig. 3(b)) characterized by three constants a, b, c and a monoclinic angle of 91.49°. In Fig. 3(b), the sublattice of $L2_1$ is displayed. The distortion plane can be viewed with atom layers A and B superimposed. The change in dimension is from length $a_0\sqrt{2}/2$ to length c for the modulation direction [110], and from $a_0\sqrt{2}/2$ to length a in the $[1\bar{1}0]$ direction. The lattice dimension in [001] is changed from $a_o$ to b. The lattice constants are summarized in Table 1. The second column gives the experimental results, while the third and fourth columns provide the simulations. The agreement between experimental and theoretical lattice constants including the monoclinic angle is remarkable. The *ab-initio* VASP code with GGA (Kresse and Furthmuller, 1996; Kresse and Hafner, 1993a,b; Kresse and Joubert, 1999) is used in the simulations (see Appendix).

Because the transformation occurs first via $L2_1 \rightarrow 10M$, we investigated the energy landscape associated with this important step. We note that the lattice parameters of the 10M are designated as $a_i, b_i, c_i$, while the $L2_1$ lattice is defined by $a_0$. Relative to the parent body the 10M phase involves a volumetric distortion and local shuffle. The deformation gradient can be written in the following form to represent the volumetric distortion, where $\varepsilon$ represents the extent of the Bain-type deformation with $\varepsilon = 0$ corresponding to the $L2_1$ and $\varepsilon = 1$ to the 10M end states. The Cauchy-Born rule was used in establishing the deformation gradient expression given below.

$$F(\varepsilon) = \begin{bmatrix} b_i(\varepsilon)/a_0\sqrt{2} & b_i(\varepsilon)/a_0\sqrt{2} & 0 \\ c_i(\varepsilon)/a_0\sqrt{2} & c_i(\varepsilon)/a_0\sqrt{2} & 0 \\ 0 & 0 & a_i(\varepsilon)/a_0\sqrt{2} \end{bmatrix} \quad (1)$$

To account for the internal displacements associated with the shuffles, the strain energy density is minimized with respect to the shuffle displacements while $F(\varepsilon)$ is held fixed. This is achieved with internal relaxations of the atoms to the local energy minimum. The normalized shuffle parameter is defined as $\eta = s/a$ where $s$ is the absolute shuffle. The energy

Please cite this article in press as: Sehitoglu, H., et al. Transformation and slip behavior of $Ni_2FeGa$. Int. J. Plasticity (2012), http://dx.doi.org/10.1016/j.ijplas.2012.05.011

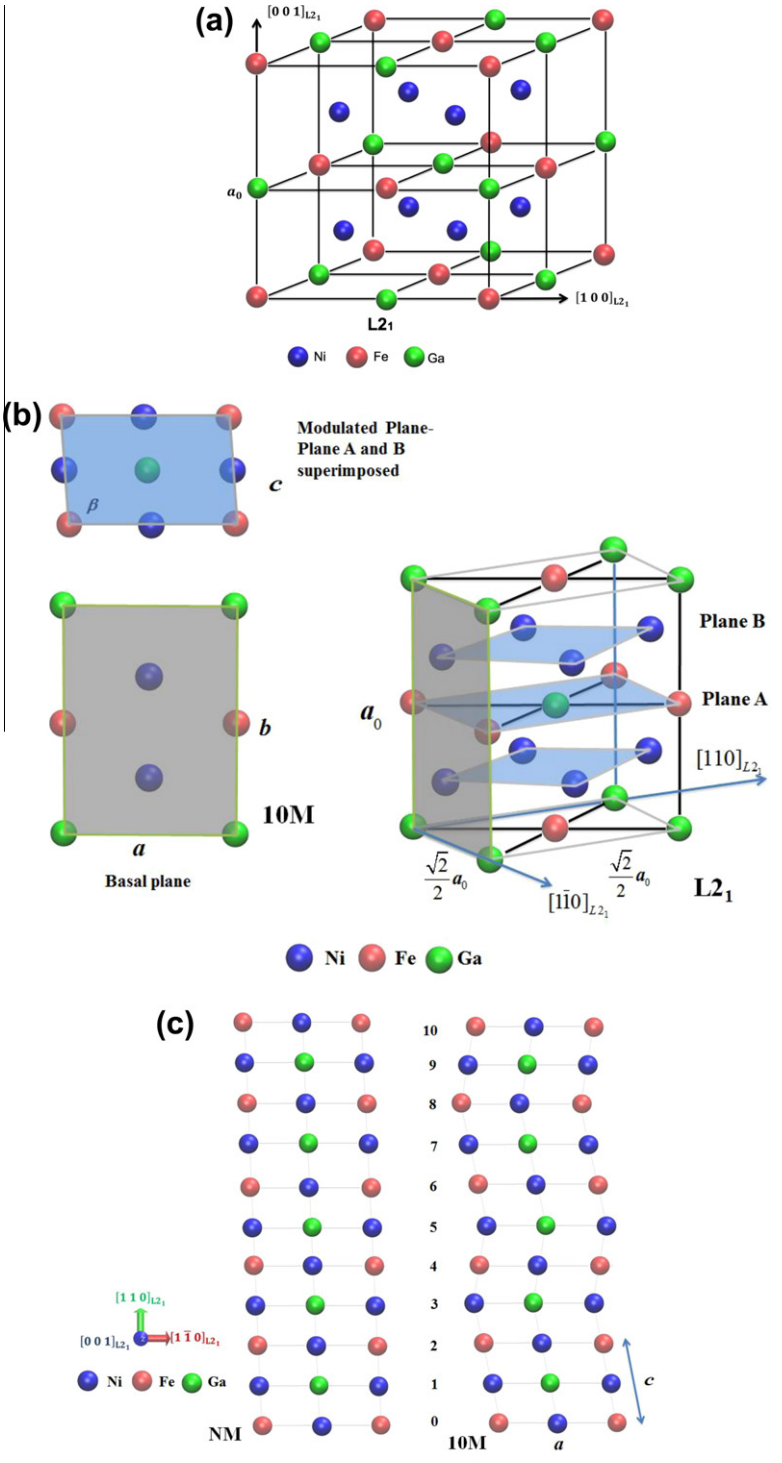


**Fig. 3.** (a) Schematic of the $L2_1$ austenitic structure of $Ni_2FeGa$, (b) the sublattice displaying the modulated and basal planes, (c) the 10M monoclinic modulated structure of Ni–Fe–Ga.

landscape is completed for the multiple pathways that could achieve $L2_1 \rightarrow 10M$ by exploring all combinations of distortion and shuffle for $Ni_2FeGa$. The transformation path to the 10M structure is rather complex as shown in Fig. 4(a) and (b) and involves both shear (Bain strain) and shuffle. The energy contours shown in Fig. 4(b) show that the non-modulated martensite (10NM) has a higher energy than the modulated 10M structure. The 10NM structure has the same lattice constants as

**Table 1**
The $L2_1$ structure lattice constants for austenitic Ni–Fe–Ga ($a_o$) and the lattice constants of the modulated monoclinic (10M) structure.

| | Experiment | Theory (this study) | |
|---|---|---|---|
| Austenite ($L2_1$) cubic structure | Lattice parameter, $a_o$ (Å), 5.76 (Sutou et al., 2004), 5.7405 (Liu et al., 2003) | Lattice parameter, $a_o$ (Å), 5.755 | Energy (eV/atom) −5.7185 |
| Martensite (10M) monoclinic structure | Lattice parameter (Å), $a$ = 4.24, $b$ = 5.38, $c$ = 4.176, (Sutou et al., 2004) Monoclinic angle = 91.49° | Lattice parameter (Å), $a$ = 4.203, $b$ = 5.434, $c$ = 4.1736 Monoclinic angle = 91.456° | −5.7206 Energy Barrier (TS) 8.5 mJ/m$^2$ |

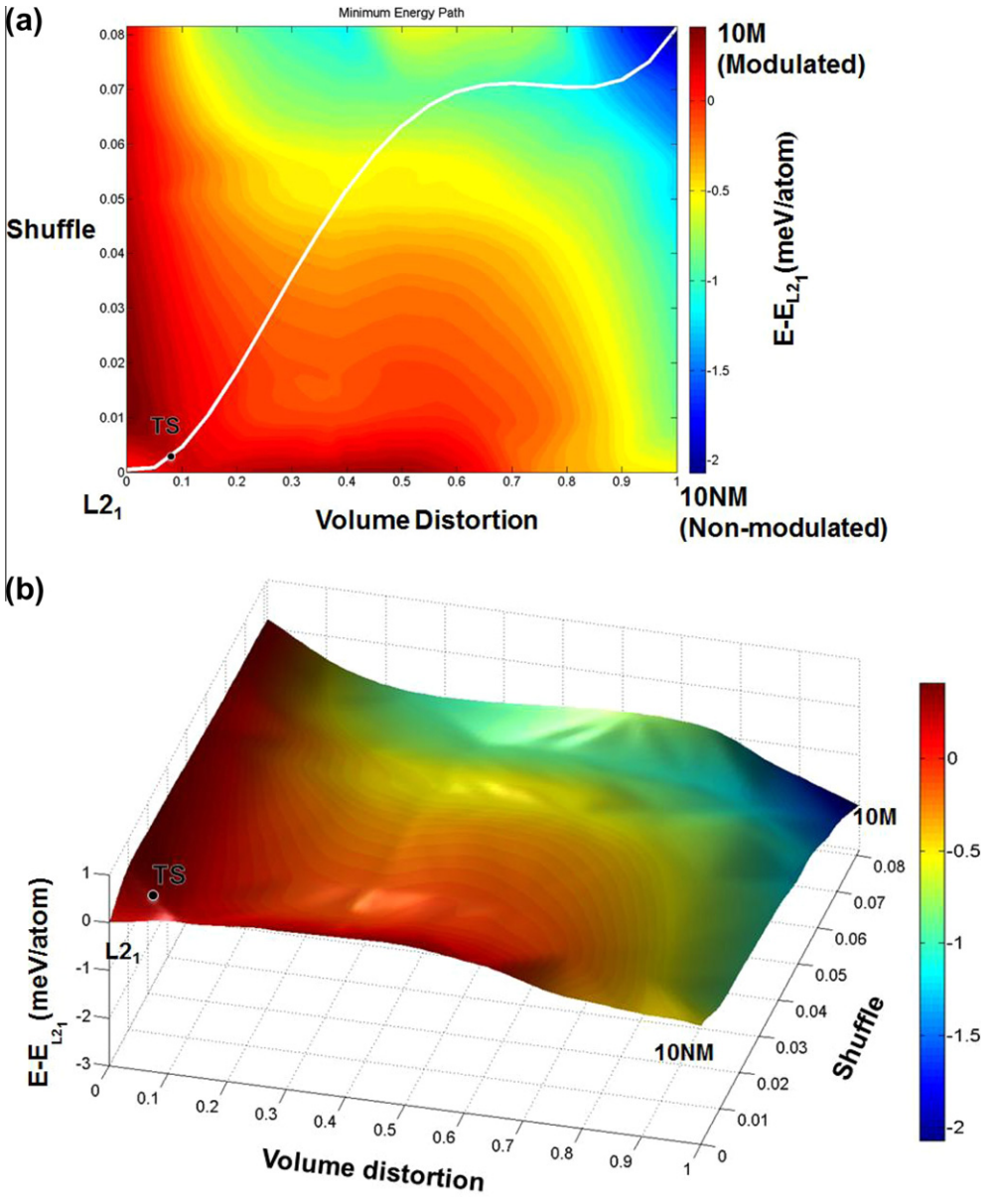


**Fig. 4.** (a) The energy landscape associated with the $L2_1$ to 10M transformation. The transformation is comprised of a distortion and shuffle and the path is rather complex. (b) 3D view of the transformation surface showing that the energy of 10NM (non-modulated martensite) structure is higher than 10M (modulated). See Fig. 3(b) for the lattices.

10M. The difference between the two is that 10M involves considerable shuffle that results in the modulation. The minimum energy path is indicated in Fig. 4(a). We note that there is a rather small barrier (8.5 mJ/m$^2$) at the early stages of combined shear and shuffle. This is the principal reason why the transformation stress is rather low (<50 MPa) in this alloy.

Please cite this article in press as: Sehitoglu, H., et al. Transformation and slip behavior of $Ni_2FeGa$. Int. J. Plasticity (2012), http://dx.doi.org/10.1016/j.ijplas.2012.05.011

To obtain the Potential Energy Surface (PES) within reasonable computational time, we divided the shear and shuffle based computational domain primarily into 7 × 7 nodes. Additional nodes are added near the energetically significant positions such as the local minima and the saddle point. A symmetry-adapted "free energy" polynomial was fitted to our $\Delta E(\eta,\varepsilon)$ data. For this fault energy functional $\Delta E(\eta,\varepsilon)$, we chose a fourth order cosine-sine polynomial (Liu and Johnson, 2009), which can appropriately represent the shear shuffle coupling, i.e.

$$\Delta E(\eta,\varepsilon)=\sum_{m,n=0}^{m+n\leqslant 4} a_{mn}[X(\eta)]^m[X(\varepsilon)]^n[1-\delta_{m0}\delta_{n0}]+\sum_{m,n=0}^{m+n\leqslant 4} b_{mn}[X(\eta)]^m[X(\varepsilon)]^n \tag{2}$$

where $[X(x)]=[1-Cos(\pi x)]$, $[Y(x)]=[Sin(\pi x)]$, and $\delta_{ij}$ represents Kronecker's delta ($\delta_{ij}$ is 1(0) if i is (not) equal to j). An additional constraint of $|d\Delta E(\eta,\varepsilon)/dx|_{x=0,1}=0$ was imposed to ensure local minima at (0,0) and (1,1) positions in the PES.

## 3. Dislocation slip (GSFE) in $Ni_2FeGa$

### 3.1. The (011)<111> case

The generalized stacking fault energy (GSFE), first introduced by Vitek (1968), is a comprehensive definition of the fault energy associated with dislocation motion. In fcc alloys, a single layer intrinsic stacking fault is formed by the passage of partial dislocations in the $<11\bar{2}>$ direction on the {111} plane. The fault energy of different sheared lattice configurations can be computed as a function of displacement $u_x$. The generalized stacking fault energy (GSFE) is represented by a surface ($\gamma$-surface) or a curve ($\gamma$-curve). The peak in fault energy was termed as the unstable SFE by Rice (1992). In the case of $Ni_2FeGa$, all fault energies are determined relative to the energy of the $L2_1$ structure.

We investigated slip in the <111> direction consistent with experiments (Chumlyakov et al., 2008). In this case the slip plane is {110}. Fig. 5(a) shows the $L2_1$ lattice with the slip plane (shaded) and the <111> direction, and Fig. 5(b) the stacking in the [111] direction as ABCDEFAB'CD'EF'..... This stacking is similar to the <111> direction in bcc metals, but the difference arises because of the presence of three elements in $Ni_2FeGa$. Because the normal plane is {112}, a total of 6 layers must be shown in this projection. The largest atom represents in-plane and the atom size becomes smaller as the out-of-plane is depicted. The smallest atom is in the fifth layer (out-of-plane) and the largest atom is in the zeroth layer (in-plane). Considerable attention should be placed on establishing the correct atom positions when multiple planes and binary or ternary alloys are considered. We utilize visualization softwares (particularly VMD) to check for accuracy of the coordinates.

We note that in the case of dislocation moving through an ordered lattice (such as $DO_3$ or $L2_1$) an antiphase boundary forms on the glide plane. The GSFE associated with the APB formation is given in Fig. 5(c). We note that the stable fault structure formed due to a shear displacement $u_x = |b|$ (see Fig. 5(c) corresponding to a local minimum, on the curve with fault energy of intrinsic stacking fault (isf) (or APB)) where $b=a_0/4[111]$ (the intrinsic stacking fault energy has been also referred as the APB energy and both terms have been used interchangeably). The equilibrium fault structure corresponds to the intrinsic stacking fault on the {110} plane. Further shear beyond the first minima on the $\gamma$-curve along <111> direction results in another stable structure at $u_x = 2|b|$ (Fig. 5(c)).

As stated earlier, the nearest neighbor (NN) and next nearest neighbor (NNN) bonds are altered in the glide plane via the passage of first partial. When the second dislocation travels in succession, it reorders the NN sites but there is a further change in the next nearest neighbor (NNN) sites. The passage of the third dislocation disorders the NN sites and results in another change of the NNN sites. The fourth dislocation reorders both the NN and NNN sites across the slip plane. If four dislocations travel in succession (as in the present case), the dislocations are bound by two types of anti-phase boundaries. Then, the distances between dislocations 1 and 2 and 2 and 3 are dictated by the APB energies ($\gamma_{NN}$ and $\gamma_{NNN}$). We note that mechanical relaxation was allowed for deviation from the perfect crystallographic displacements and these displacements were found to be less than 1% of the Burgers vector (Paidar, 1973; Yamagiuchi et al., 1981). Although these displacements are small, the relaxation in all three directions permits higher accuracy in terms of the APB energy values (Fig. 5(c)).

The position of the atoms corresponding to $b=a_0/4[111]$ is shown in Fig. 6(a). The ordering is incorrect across AD,BE,DC, DA ..... planes. We note that in Fig. 6(b) the correct ordering has been restored connecting the atoms across AA,CC, and EE. Thus, the NNNAPB plane is subdivided periodically with all Ni atoms arranged in the original ordered positions along $[1\bar{1}0]$ direction, with the adjacent layers of Fe and Ga not conforming to the original order.

The superdislocation splitting into four superpartials with two NN APBs and one NNN APB can be described as,

$$[111]=1/4[111]+NNAPB+1/4[111]+NNNAPB+1/4[111]+NNAPB+1/4[111]$$

where the lattice constant is omitted in the expression. The APBs pull the partials together while their elastic interaction results in repulsion. There is equilibrium spacing for the APB boundaries. Ribbons of APB formed by dislocation glide are visible as bands in transmission electron microscopy of deformed samples which we discuss below.

The separations of the partial dislocations $d_1$ and $d_2$ can be calculated using force balance (Crawford et al., 1973; Stroh, 1958) for each partial leading to the following equations:

Please cite this article in press as: Sehitoglu, H., et al. Transformation and slip behavior of $Ni_2FeGa$. Int. J. Plasticity (2012), http://dx.doi.org/10.1016/j.ijplas.2012.05.011

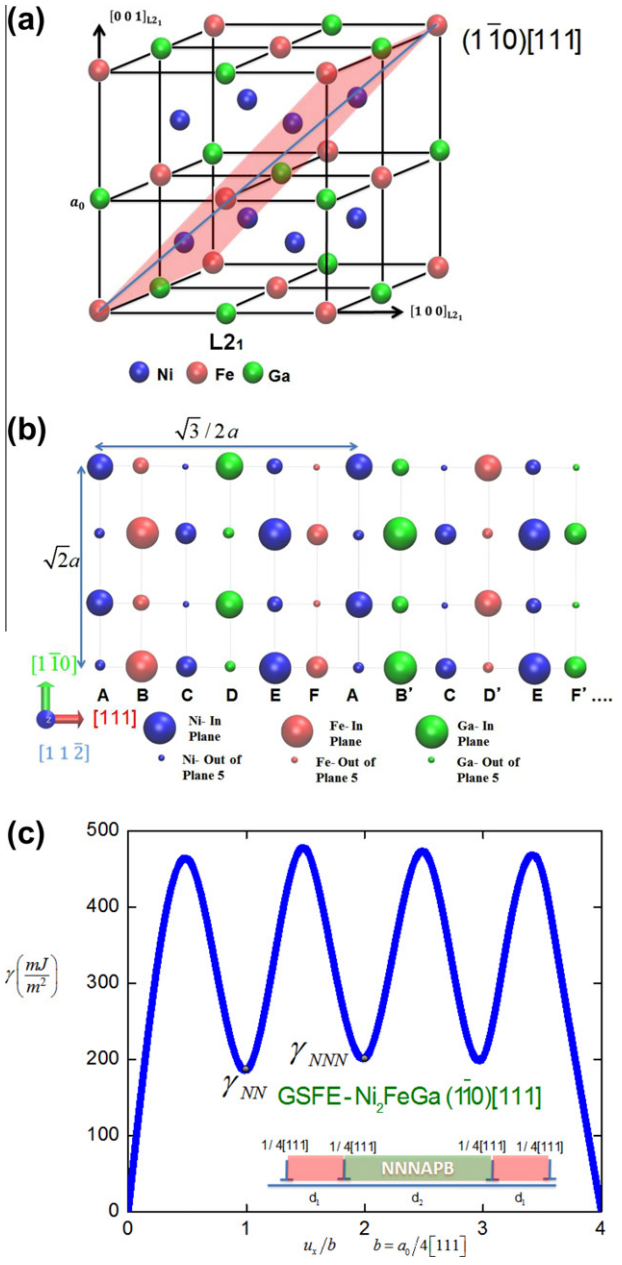


**Fig. 5.** (a) The austenite ($L2_1$) lattice showing the slip plane and slip direction, (b) the {112} projection illustrating the atom positions on the {110} plane and <111> direction, note the stacking sequence in the [111] direction, (c) upon shearing in the <111> direction the dissociation of the superlattice dislocation $a_o[111]$ to four partials, and the associated NNAPB and NNNAPB energies are noted.

$$\gamma_{NN} = K\{\frac{1}{d_1} + \frac{1}{d_1 + d_2} + \frac{1}{2d_1 + d_2}\}$$
$$\gamma_{NNN} - \gamma_{NN} = K\{\frac{1}{d_2} + \frac{1}{d_1 + d_2} - \frac{1}{d_1}\}$$

These equations can be solved for the separation distances giving the energy levels and the other material constants as input. The factor K is given as $K = \frac{\mu b_p^2}{2\pi}$ where μ = 19 Gpa (obtained from our simulations), $b_p = \frac{\sqrt{3}a_0}{4}$ and $a_0$ = 5.755 Å as noted earlier. This results in $d_1 = 1.73$ nm, $d_2 = 2.41$ nm, hence the width of the entire fault is of the order of 10 $a_0$. We note that if the shear modulus is not known from simulations one can determine the value of $K$ above from the cubic constants using a formula provided by Head (1964).

Please cite this article in press as: Sehitoglu, H., et al. Transformation and slip behavior of $Ni_2FeGa$. Int. J. Plasticity (2012), http://dx.doi.org/10.1016/j.ijplas.2012.05.011

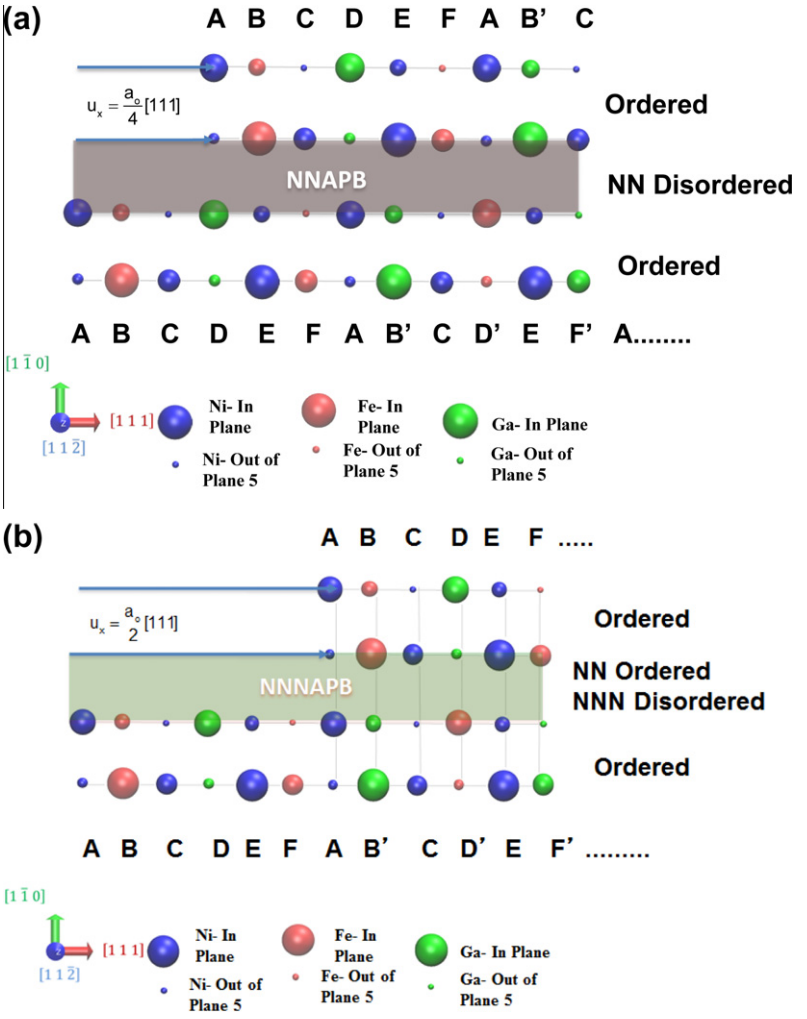


**Fig. 6.** (a) Atomic displacements for $Ni_2FeGa$ along the [111] direction. The atoms across the slip plane with a basic displacement of 1/4[111] are no longer in the correct position, (b) upon a displacement of 1/2[111] atoms AA, CC, EE across the slip plane (APB) are partially ordered.

### *3.2. The (011) <001> case*

We conducted simulations to determine the energy barriers (GSFE) for the (011) <111> dislocation slip. The (011) <111> dislocation slip system has been observed experimentally for CuZnAl alloys as mentioned earlier. As the ionic character of the bonding changes there is a transition to <100> slip as noted for NiTi (Rachinger, 1956). Therefore, it is important to check the GSFE behavior and compare the results to the <111> case.

The atomic configuration for our simulations is shown in Fig. 7(a). The GSFE results are given in Fig. 7(b). We note the stacking fault energy is near 250 mJ/m$^2$. Most importantly, the unstable energy barrier is very high near 1400 mJ/m$^2$. The full dislocation dissociated to ½[001] in this case. The stress level required to overcome the unstable barrier is rather high in this case, hence this slip system would require very high stress magnitudes to be activated in $Ni_2FeGa$.

## 4. Experimental results

Single crystal $Ni_{54}Fe_{19}Ga_{27}$ with [0 01] orientation was utilized in this work. After single crystal growth, the samples were heat treated at 900 °C for 3 h and subsequently water quenched. The details of the processing and heat treatment are described in our previous work (Hamilton et al., 2006). The $Ni_2FeGa$ is characterized by the forward and reverse transformation temperatures obtained via differential scanning calorimetry. The reverse transformation temperature (martensite to austenite) for the Ni-Fe–Ga alloy is 16 °C. Our experiments were conducted at room temperature (25 °C). The material is in the austenitic state at the beginning of the experiment and undergoes a stress-induced transformation. In the first step the transformation is from $L2_1$ to 10M with a transformation strain of 4%, then transformation to 14M results in additional 2% strain.

Please cite this article in press as: Sehitoglu, H., et al. Transformation and slip behavior of $Ni_2FeGa$. Int. J. Plasticity (2012), http://dx.doi.org/10.1016/j.ijplas.2012.05.011

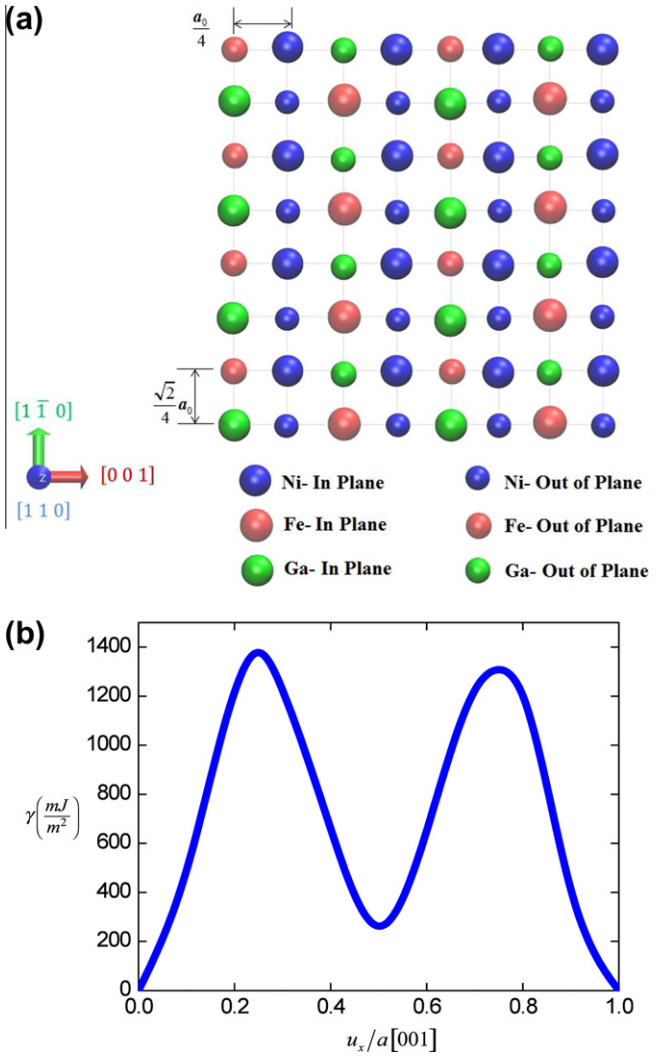


**Fig. 7.** (a) Atomic configuration for the (011) <100> slip, (b) the GSFE curve for the (011) <100> case.

Finally, the transformation to $L1_0$ (tetragonal) results in a transformation strain as high as 12%. Single crystals (of [001] direction) were used in the experiments to facilitate the interpretation of results and maximize the transformation strains. The samples were deformed to a strain of 12% and then unloaded to zero strain. This process was repeated and pseudoelastic behavior was established cycle after cycle. The stress-strain response is shown in Fig. 8(a).

Digital image correlation results (DIC) providing for the strain fields are given in Fig. 8(a). The initial transformation stress represents the $L2_1$ to 10M transformation. The details of the DIC technique for measuring the displacement fields by tracking features on the specimen surface can be found in Efstathiou et al. (2010). The DIC local strain measurement images are shown at selected points along the curve for the $Ni_2FeGa$ alloy. Each image in the figure corresponds to a marker point indicated on the stress-strain curve. Note that the loading axis for all images is vertical, and the color contours represent magnitudes of axial strain based on the inset common scale. With proper choice of magnification, nuances of martensite nucleation and strain gradients at austenite/martensite interfaces can be resolved.

As the loading reaches a critical transformation stress, one can establish the instant of martensite nucleation and the corresponding stress precisely. In the third image of the sequence (left to right), the 10M phase appears as the blue region and this 10M band propagates along the specimen length. This shows that it is possible to identify intermediate transformations not evident in the macroscale stress-strain response. With further deformation, a critical transformation stress for the $L1_0$ phase is achieved at approximately 80 MPa and followed by a second plateau.

Under suitable composition and annealing conditions, second-phase ($\gamma$-phase) particles with a FCC structure can be precipitated in the $L2_1$ austenite of $Ni_2FeGa$. Based on the Fe content determined by Energy-dispersive X-ray spectroscopy (EDX), this phase does not undergo a martensitic transformation, but plastic accommodation (Hamilton et al., 2007b; Omori

Please cite this article in press as: Sehitoglu, H., et al. Transformation and slip behavior of $Ni_2FeGa$. Int. J. Plasticity (2012), http://dx.doi.org/10.1016/j.ijplas.2012.05.011

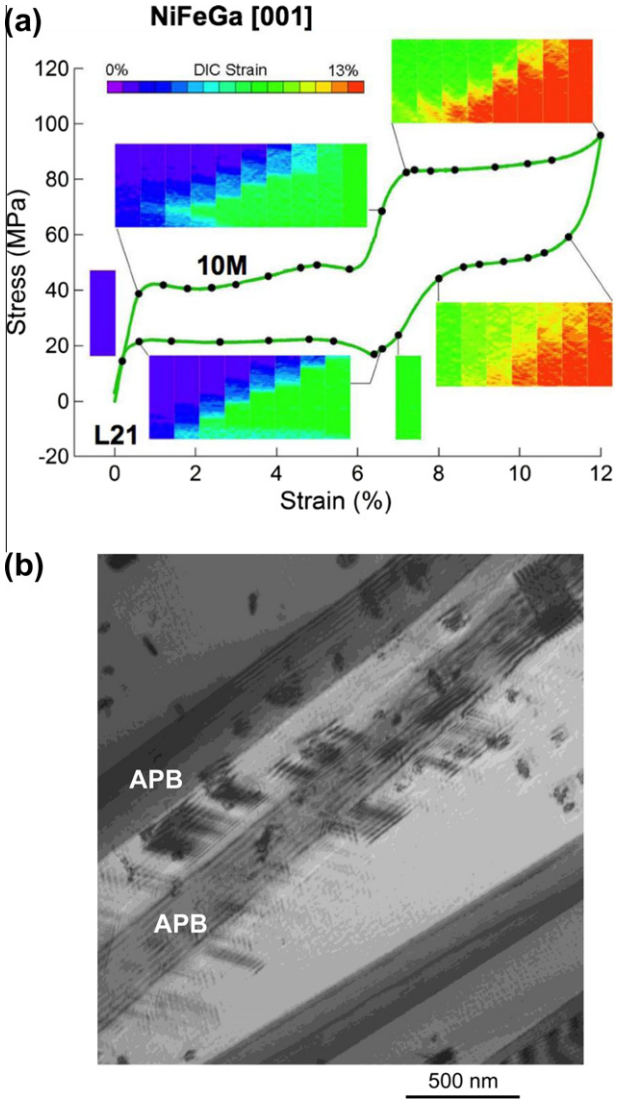


**Fig. 8.** (a) Pseudoelasticity experiments (at room temperature) (Efstathiou et al., 2008) and (b) TEM results displaying APBs in the austenite domains.

et al., 2004). In Fig. 8(b), the TEM results are shown clearly displaying the presence of APBs in this alloy. The TEM samples were extracted from samples that have undergone pseudoelastic cycling as described above. The dislocations were retained after the cycling sequence. The APBs appear as series of lines and are extended across the specimen width. Considering some deviations because of magnetic rotation between diffraction patterns and the actual image, the trace of the image was found to be close to the {110} type plane.

## 5. Implication of Results

Based on the GSFE results the ideal stress levels for dislocation slip were calculated for <111> and <001> directions and the magnitudes are shown in Table 2. We note that the stress magnitudes for slip nucleation, $(\tau_{\text{shear}})_{nuc} = \frac{\delta\gamma}{\delta u_x}\Big|$, are rather high precluding significant slip within austenite. However, the stresses at the austenite -martensite interfaces can be sufficiently high to generate dislocation slip in the austenite domains. Furthermore, Fisher (1954) made a first order estimate of the additional stress associated with the dislocation motion creating a change in order within the crystal. The increase in energy of the interface needs to be balanced by the extra applied shear stress to move the dislocations. Upon utilizing 200 mJ/m$^2$ (corresponding to the lower value of $\gamma_{NN}$) we calculate the Fisher strengthening to be near 1 GPa for both cases as shown in Table 2.

We finally note that the calculated separation distances for partials within the APBs are consistent with the experiments reported in this study. The precise width of the APBs can be further resolved by experiment utilizing high resolution methods, which are outside the scope of the present work. Even though the experimental measurement of separation distances is

Please cite this article in press as: Sehitoglu, H., et al. Transformation and slip behavior of $Ni_2FeGa$. Int. J. Plasticity (2012), http://dx.doi.org/10.1016/j.ijplas.2012.05.011

**Table 2**
Calculated fault energies, Burgers vector, (ideal) critical stress for slip nucleation and Fisher stress for movement of APBs.

| Slip plane | Slip direction | Theory (this study) | | | |
|---|---|---|---|---|---|
| | | $b$ (Å) | $\gamma$, Fault energy (mJ/m$^2$) | $(\tau_{shear})_{nuc} = \frac{\delta\gamma}{\delta u_x}$ (GPa) | $(\tau_{shear})_F = \frac{\gamma}{b}$ (GPa) |
| $(1\bar{1}0)$ | [111] | 2.5 | 200 | 3.7 | 0.8 |
| $(1\bar{1}0)$ | [001] | 2.88 | 263 | 9.5 | 0.9 |

not available because they are only several nanometers, the experiments clearly show the presence of APBs. An example of high density of APB formation in Ni–Fe–Ga has also been reported by Chumlyakov et al. (2008) and the images are in agreement to those presented in this study.

We make a comparison between the current results and the work on CuZnAl alloys where the fault energies were of the order of 45 mJ/m$^2$, which resulted in prediction of Fisher strengthening near 330 MPa (Romero et al., 1988). Similarly, if we are to consider dislocation glide in $Ni_2FeGa$ and use Fisher's formula ($(\tau_{shear})_F$) we find the magnitude of extra shear stress to drag the APBs to be near 0.8–0.9 GPa. This magnitude is still significantly higher than the transformation stresses (less than 0.2 GPa) observed experimentally for $Ni_2FeGa$. Taking into account the temperature dependence in the phase transformation and plasticity behavior, we note that the critical stresses for the initial martensitic transformation and slip nucleation in $Ni_2FeGa$ will be modified with increasing temperatures. However, the present results are insightful because they represent the energies associated with displacements to render the transformation or plasticity at a reference temperature (0K). Consequently, there is mounting evidence of the potential for $Ni_2FeGa$ as a shape memory alloy with favorable characteristics. To our knowledge, this is the first time the transformation path for $L2_1$ to 10M for $Ni_2FeGa$ has been determined and the GSFE in <111> and <001> directions are computed for the same alloy. Also, we present experimental evidence of APBs for samples that have undergone pseudoelastic cycling.

There are a number of reasons why a transformation is reversible versus irreversible. Reversibility is favored when the energy barriers for forward and reverse transformations are small compared to the energy barriers for dislocation slip. The absence of long range ordering results in rather large hysteresis levels in martensite transformations. For example, the Fe–C or Fe–Ni steels exhibit very large thermal hysteresis of the order of 400 °C, and the FeNiCoTi and FeMnSi fcc shape memory alloys (which do not have long-range ordering) also exhibit high hysteresis levels (200 °C). On the other hand, the Fe–Pt shape memory alloys, which can be ordered (Foos et al., 1977), exhibit hysteresis levels as low as 10 °C. In Ni based alloys (also of the shape memory variety) such as NiTi, NiTiX (X = Cu, Fe), where long-range ordered B2 to monoclinic martensite transformation has been observed, the hysteresis levels are typically of the order of 10 °C to 20 °C. In $Ni_2FeGa$, where the austenite phase is long-range ordered cubic $L2_1$ and the martensite is monoclinic 10M, the thermal hysteresis can be as low as 1 °C (Hamilton et al., 2007a) generating new possibilities for applications (Pons et al., 2008). It is shown that the transformation barrier is rather low in $Ni_2FeGa$ (8.5 mJ/m$^2$), hence the critical stress levels for forward and reverse transformation are much lower than for dislocation slip.

There has been previous discussion of the slip systems in $L2_1$ shape memory alloys of the CuZnAl type. The <111> glide planes have been observed with APB formation for the $L2_1$ CuZnAl alloys as well (Damiani et al., 2002a; Romero et al., 1988). It is known that when the APB energies are low, <111> slip dominates. As APB energies become higher with increasing ionic character, <100> slip is favored as noted by Rachinger and Cottrell (Rachinger, 1956). The present results show that the unstable energies for the <001> case are exceedingly high precluding its occurrence unless the stress magnitudes exceed a few GPa.

Finally, we summarize what primarily influences the transformation reversibility of $Ni_2FeGa$ alloys. The increase in elastic accommodation of the transformation with an increase in plastic slip resistance leads to the reversible transformations. We show that the slip resistance in long-ranged ordered $Ni_2FeGa$ is high with total dislocations decomposing to partials connected with anti-phase boundaries.

## Acknowledgements

The work was supported by the NSF grant CMMI-09-26813 and partly by DMR-08-03270.

## Appendix A

The first-principles total-energy calculations were carried out using the Vienna ab initio Simulations Package (VASP) with the projector augmented wave (PAW) method and the generalized gradient approximation (GGA). In our calculation, we used a $9 \times 9 \times 9$ Monkhorst Pack k-point meshes for the Brillouin-zone integration to ensure the convergence of results. The energy cut-off of 500 eV was used for the plane-wave basis set. The total energy was converged to less than 10-5 eV per atom. Considering the effect of the number of layers on stacking fault energies (Hatcher et al., 2009), the present DFT calculation of GSFE for slip system (011)<111> is conducted using a 8 layer supercell having 12-atom per layer; while for slip system (011)<001>, a 8 layer supercell having 4-atom per layer is used. For every shear displacement, the relaxation

perpendicular to the fault plane was allowed for minimizing the short-range repulsive energy between misfitted adjacent layers (Fu and Yoo, 1992; Paidar, 1976). We construct a supercell consisting of 40 atoms to model the 10M structure in order to incorporate the full period of modulation in the supercell (Luo et al., 2011a; Zayak et al., 2005). The relaxation by changing the supercell shape, volume and atomic positions were carried out. The periodic boundary conditions are maintained across the supercell to represent bulk Ni2FeGa material (no free surface). All supercells used in the study ensure the convergence of the calculation after careful testing.

The lattice parameters of $L2_1$ and $L1_0$ structures using DFT were calculated and compared with experimental measurements. They are in a good agreement. In order to obtain the 10M structure, the initial calculation parameters $a = 4.272$ Å, $b = 5.245$ Å, $c = 4.25$ Å and the monoclinic angle $\beta = 91.49°$ (Sutou et al., 2004) are estimated by assuming the lattice correspondence with the $L1_0$ structure (Kainuma et al., 1996; Ryosuke et al., 2000). The relaxation by changing the supercell shape, volume and atomic positions were carried out. By using this optimization method, the atoms in the supercell move from their initial positions after each relaxation step by local forces, and after numerous such iteration processes, the configuration will be finally converged where the forces are zero in the stable 10M structure.

## References

Ahlers, M., 2002. The martensitic transformation: Mechanisms and crystallography. Philosophical Magazine A 82, 1093–1114.
Bartel, T., Menzel, A., Svendsen, B., 2011. Thermodynamic and relaxation-based modeling of the interaction between martensitic phase transformations and plasticity. Journal of the Mechanics and Physics of Solids 59, 1004–1019.
Boyd, J.G., Lagoudas, D.C., 1996. A thermodynamical constitutive model for shape memory materials. Part I. The monolithic shape memory alloy. International Journal of Plasticity 12, 805–842.
Chumlyakov, Y., Kireeva, I., Panchenko, E., Timofeeva, E., Pobedennaya, Z., Chusov, S., Karaman, I., Maier, H., Cesari, E., Kirillov, V., 2008. High-temperature superelasticity in CoNiGa, CoNiAl, NiFeGa, and TiNi monocrystals. Russian Physics Journal 51, 1016–1036.
Crawford, R.C., Ray, I.L.F., Cockayne, D.J.H., 1973. The weak-beam technique applied to superlattice dislocations in iron-aluminium alloys. Philosophical Magazine 27, 1–7.
Damiani, C., Lovey, F.C., Sade, M., 2002a. Plastic deformation under compression of Cu-Zn-Al martensitic single crystals. Materials Science and Engineering A 323, 436–444.
Damiani, C., Lovey, F.C., Sade, M., 2002b. Plastic deformation under compression of Cu-Zn-Al martensitic single crystals. Materials Science & Engineering A (Structural Materials: Properties, Microstructure and Processing) A323, 436–444.
Delaey, L., Krishnan, R.V., Tas, H., Warlimont, H., 1974. Thermoelasticity, pseudoelasticity and the memory effects associated with martensitic transformations. Journal of Materials Science 9, 1521–1535.
T.W. Duerig, K.N.M., D. Stöckel, C.M. Wayman, Editors, 1990. Engineering Aspects of Shape Memory Alloys,. Butterworth-Heinemann, Boston.
Efstathiou, C., Sehitoglu, H., Carroll, J., Lambros, J., Maier, H.J., 2008. Full-field strain evolution during intermartensitic transformations in single-crystal NiFeGa. Acta Materialia 56, 3791–3799.
Efstathiou, C., Sehitoglu, H., Lambros, J., 2010. Multiscale strain measurements of plastically deforming polycrystalline titanium: Role of deformation heterogeneities. International Journal of Plasticity 26, 93.
Ezaz, T., Sehitoglu, H., Maier, H.J., 2011. Energetics of twinning in martensitic NiTi. Acta Materialia 59, 5893–5904.
Fisher, J.C., 1954. On the strength of solid solution alloys. Acta Metallurgica 2, 9–10.
Foos, M., Frantz, C., Durupt, S., Gavoille, G., 1977. On reversible shape memory effect related to microstructural memory and residual stresses in Fe3Pt. Scripta Metallurgica 11, 655–658.
Fu, C.L., Yoo, M.H., 1992. Deformation behavior of B2 type aluminides: FeAl and NiAl. Acta Metallurgica et Materialia 40, 703–711.
Hamilton, R.F., Sehitoglu, H., Chumlyakov, Y., Maier, H.J., 2004. Stress dependence of the hysteresis in single crystal NiTi alloys. Acta Materialia 52, 3383.
Hamilton, R.F., Efstathiou, C., Sehitoglu, H., Chumlyakov, Y., 2006. Thermal and stress-induced martensitic transformations in NiFeGa single crystals under tension and compression. Scripta Materialia 54, 465.
Hamilton, R.F., Sehitoglu, H., Efstathiou, C., Maier, H.J., 2007a. Inter-martensitic transitions in Ni-Fe–Ga single crystals. Acta Materialia 55, 4867–4876.
Hamilton, R.F., Sehitoglu, H., Efstathiou, C., Maier, H.J., 2007b. Mechanical response of NiFeGa alloys containing second-phase particles. Scripta Materialia 57, 497–499.
Han, M., Bennett, J.C., Gharghouri, M.A., Chen, J., Hyatt, C.V., 2007. Understanding modulated twin transition at the atomic level. Acta Materialia 55, 1731–1740.
Hatcher, N., Kontsevoi, O.Y., Freeman, A.J., 2009. Role of elastic and shear stabilities in the martensitic transformation path of NiTi. Physical Review B (Condensed Matter and Materials Physics) 80, 144203 (144218 pp.).
Head, A.K., 1964. The [111] Dislocation in a Cubic Crystal. physica status solidi (b) 6, 461–465.
Idesman, A.V., Levitas, V.I., Stein, E., 2000. Structural changes in elastoplastic material: a unified finite-element approach to phase transformation, twinning and fracture. International Journal of Plasticity 16, 893–949.
Kainuma, R., Nakano, H., Ishida, K., 1996. Martensitic transformations in NiMnAl β phase alloys. Metallurgical and Materials Transactions A: Physical Metallurgy and Materials Science 27A, 4153–4162.
Kibey, S., Sehitoglu, H., Johnson, D.D., 2009. Energy landscape for martensitic phase transformation in shape memory NiTi. Acta Materialia 57, 1624.
Koehler, J.S., Seitz, F., 1947. Proposed experiments for further study of mechanism of plastic deformation. American Society of Mechanical Engineers –. Journal of Applied Mechanics 14, 217–224.
Kresse, G., Furthmuller, J., 1996. Efficient iterative schemes for ab initio total-energy calculations using a plane-wave basis set. Physical Review B (Condensed Matter) 54, 11169.
Kresse, G., Hafner, J., 1993a. Ab initio Hellmann-Feynman molecular dynamics for liquid metals, Netherlands, p. 956.
Kresse, G., Hafner, J., 1993b. Ab initio molecular dynamics for open-shell transition metals. Physical Review B (Condensed Matter) 48, 13115.
Kresse, G., Joubert, D., 1999. From ultrasoft pseudopotentials to the projector augmented-wave method. Physical Review B (Condensed Matter) 59, 1758.
Levitas, V.I., 2002. Critical thought experiment to choose the driving force for interface propagation in inelastic materials. International Journal of Plasticity 18, 1499–1525.
Liu, J.B., Johnson, D.D., 2009. Bcc-to-hcp transformation pathways for iron versus hydrostatic pressure: Coupled shuffle and shear modes. Physical Review B 79, 134113.
Liu, Z.H., Zhang, M., Cui, Y.T., Zhou, Y.Q., Wang, W.H., Wu, G.H., Zhang, X.X., Xiao, G., 2003. Martensitic transformation and shape memory effect in ferromagnetic Heusler alloy Ni[sub 2]FeGa. Applied Physics Letters 82, 424–426.
Luo, H.B., Li, C.M., Hu, Q.M., Kulkova, S.E., Johansson, B., Vitos, L., Yang, R., 2011a. First-principles investigations of the five-layer modulated martensitic structure in Ni2Mn(AlxGa1−x) alloys. Acta Materialia 59, 5938–5945.
Luo, H.B., Li, C.M., Hu, Q.M., Kulkova, S.E., Johansson, B., Vitos, L., Yang, R., 2011b. First-principles investigations of the five-layer modulated martensitic structure in Ni 2Mn(Al xGa 1-x) alloys. Acta Materialia 59, 5938–5945.

Please cite this article in press as: Sehitoglu, H., et al. Transformation and slip behavior of $Ni_2FeGa$. Int. J. Plasticity (2012), http://dx.doi.org/10.1016/j.ijplas.2012.05.011

Maki, T., 1998a. Improvement of shape memory effect in Fe–Mn–Si alloys by strengthening of austenite matrix, International Conference on Displacive Phase Transformations and their Applications in Materials Engineering. In: Honor of Professor CM Wayman on the Occasion of His Retirement, 8–9 May 1996. TMS, Warrendale, PA, USA, pp. 111–117.
Maki, T., 1998b. Improvement of shape memory effect in Fe-Mn-Si alloys by strengthening of austenite matrix, Proceedings of the 1996 International Conference on Displacive Phase Transformations and their Applications in Materials Engineering, May 8, 1996 - May 9, 1996. Minerals, Metals & Materials Soc (TMS), Urban, IL, USA, pp. 111-117.
Malarria, J., Lovey, F.C., Sade, M., 2009. Two way shape memory effect in CuZnAl single crystals after pseudoelastic cycling at low temperatures. Materials Science & Engineering: A (Structural Materials: Properties, Microstructure and Processing) 517, 118–124.
Manchiraju, S., Anderson, P.M., 2010. Coupling between martensitic phase transformations and plasticity: A microstructure-based finite element model. International Journal of Plasticity 26, 1508–1526.
Marcinkowski, M.J., Brown, N., 1961. Theory and direct observation of dislocations in the Fe3Al superlattices. Acta Metallurgica 9, 764–786.
Martynov, V.V., 1995. X-ray diffraction study of thermally and stress-induced phase transformations in single crystalline Ni–Mn–Ga alloys, C8 ed. Editions de Physique, Lausanne, Switzerland, pp. 91–99.
Masdeu, F., Pons, J., Segui, C., Cesari, E., Dutkiewicz, J., 2005. Some features of Ni–Fe–Ga shape memory alloys under compression. Journal of Magnetism and Magnetic Materials 290–291, 816.
Moberly, W.J., Proft, J.L., Duerig, T.W., Pelton, A.R., Sinclair, R., 1991. Thermomechanical strengthening of B2 intermetallics. Publ by Minerals, Metals & Materials Soc (TMS), New Orleans, LA, USA, p. 387.
Morito, S., Moritani, T., Furuhara, T., Maki, T., 2000. Martensitic transformation in thin foils of an Fe–Ni–Co–Ti shape memory alloy, International Symposium and Exhibition on Shape Memory Materials (SMM '99), 19–21 May 1999. Trans Tech Publications, Switzerland, pp. 207–210.
Morito, H., Oikawa, K., Fujita, A., Fukamichi, K., Kainuma, R., Ishida, K., 2005. Enhancement of magnetic-field-induced strain in Ni–Fe–Ga–Co Heusler alloy. Scripta Materialia 53, 1237–1240.
Jost, N., 1999. Thermal fatigue of Fe–Ni–Co–Ti shape-memory-alloys. Materials Science and Engineering A 273–275, 649–653.
Norfleet, D.M., Sarosi, P.M., Manchiraju, S., Wagner, M.F.X., Uchic, M.D., Anderson, P.M., Mills, M.J., 2009. Transformation-induced plasticity during pseudoelastic deformation in Ni-Ti microcrystals. Acta Materialia 57, 3549–3561.
Olson, G.B., Cohen, M., 1975. Thermoelastic behavior in martensitic transformations. Scripta Metallurgica 9, 1247.
Omori, T., Kamiya, N., Sutou, Y., Oikawa, K., Kainuma, R., Ishida, K., 2004. Phase transformations in Ni-Ga-Fe ferromagnetic shape memory alloys. Materials Science and Engineering A 378, 403–408.
Otsuka, K., Wayman, C.M., 1998. Shape Memory Materials. Cambridge University Press, Cambridge.
Paidar, V., 1973. The equilibrium shape of the antiphase domains in the DO3 structure. Czechoslovak Journal of Physics, Section B B23, 1231–1236.
Paidar, V., 1976. Generalized stacking faults in model lattice of ordered Fe-Si alloys. Czechoslovak Journal of Physics 26, 865–874.
Pelton, A.R., Huang, G.H., Moine, P., Sinclair, R., 2012. Effects of thermal cycling on microstructure and properties in Nitinol. Materials Science and Engineering: A 532, 130–138.
Pons, J., Cesari, E., Segu√≠, C., Masdeu, F., Santamarta, R., 2008. Ferromagnetic shape memory alloys: Alternatives to Ni, ÄìMn, ÄìGa. Materials Science and Engineering: A 481, Äì482, 57–65.
Rachinger WA, C.A., 1956. Slip in crystals of caesium chloride type.. Acta Metallurgica 4:109.
Rice, J.R., 1992. Dislocation nucleation from a crack tip: An analysis based on the Peierls concept. Journal of the Mechanics and Physics of Solids 40, 239.
Romero, R., Lovey, F., Ahlers, M., 1988. Plasticity in Œ⩽ phase Cu-Zn-Al alloys. Philosophical Magazine A 58, 881–903.
Roqueta, D.O., Lovey, F.C., Sade, M., 1997. Hysteresis evolution in the martensitic transformation cycling in -Cu-Zn-Al samples with -phase precipitates. Scripta Materialia 36, 385–391.
Ryosuke, K., Fumihiko, G., Yuji, S., Ikuo, O., Kiyohito, I., 2000. Ordering, Martensitic and Ferromagnetic Transformations in Ni-Al-Mn Heusler Shape Memory Alloys. Materials Transactions, JIM 41, 943–949.
Sade, M., Hazarabedian, A., Uribarri, A., Lovey, F.C., 1988. Effects of cycling through stress-induced martensitic transformation in Cu-Zn-Al alloys on dislocation structures and two-way memory, Phase Transformations '87. Proceedings of the Conference, 6-10 July 1987. Inst. Met, London, UK, pp. 279-281.
Santamarta, R., Cesari, E., Font, J., Muntasell, J., Pons, J., Dutkiewicz, J., 2006a. Effect of atomic order on the martensitic transformation of Ni-Fe-Ga alloys. Scripta Materialia 54, 1985–1989.
Santamarta, R., Font, J., Muntasell, J., Masdeu, F., Pons, J., Cesari, E., Dutkiewicz, J., 2006b. Effect of ageing on the martensitic transformation of Ni-Fe-Ga alloys. Scripta Materialia 54, 1105–1109.
Segui, C., Chernenko, V.A., Pons, J., Cesari, E., Khovailo, V., Takagi, T., 2005. Low temperature-induced intermartensitic phase transformations in Ni-Mn-Ga single crystal. Acta Materialia 53, 111–120.
Sehitoglu, H., Karaman, I., Anderson, R., Zhang, X., Gall, K., Maier, H.J., Chumlyakov, Y., 2000. Compressive response of NiTi single crystals. Acta Materialia 48, 3311–3326.
Simon, T., Kroger, A., Somsen, C., Dlouhy, A., Eggeler, G., 2010. On the multiplication of dislocations during martensitic transformations in NiTi shape memory alloys. Acta Materialia 58, 1850–1860.
Sittner, P., Novak, V., Zarubova, N., 1998. Martensitic transformations in [001] CuAlZnMn single crystals. Acta Materialia 46, 1265–1281.
Stroh, A.N., 1958. Dislocations and Cracks in Anisotropic Elasticity. Philosophical Magazine 3, 625–646.
Sutou, Y., Kamiya, N., Omori, T., Kainuma, R., Ishida, K., Oikawa, K., 2004. Stress-strain characteristics in Ni-Ga-Fe ferromagnetic shape memory alloys. Applied Physics Letters 84, 1275.
Tsuzaki, K., Ikegami, M., Tomota, Y., Kurokawa, Y., Nakagawa, W., Maki, T., 1992. Effect of thermal cycling on the martensitic transformation in an Fe-24Mn-6Si shape memory alloy. Materials Transactions, JIM 33, 263–270.
Vitek, V., 1968. Intrinsic stacking faults in body-centred cubic crystals. Philosophical Magazine 18, 773–786.
Wagner, M.F.X., Windl, W., 2008. Lattice stability, elastic constants and macroscopic moduli of NiTi martensites from first principles. Acta Materialia 56, 6232.
Wechsler, M.S., Lieberman, D.S., Read, T.A., 1953. On theory of formation of martensite. Journal of Metals 5, 1503–1515.
Yamagiuchi, M., Pope, D.P., Vitek, V., Umakoshi, Y., 1981. Planar faults and dislocation dissociations in body-centred-cubic-derivative ordered structures. Philosophical Magazine A 43, 1265–1275.
Zayak, A., Adeagbo, W.A., Entel, P., Buchelnikov, V.D., 2005. Crystal structures of Ni2MnGa from density functional calculations. Phase Transitions 78, 259–266.

Please cite this article in press as: Sehitoglu, H., et al. Transformation and slip behavior of $Ni_2FeGa$. Int. J. Plasticity (2012), http://dx.doi.org/10.1016/j.ijplas.2012.05.011